J Geophys (1986) 59:73–86

Journal of Geophysics

Electric fields and currents at the Harang discontinuity: a case study

T. Kunkel[1]*, W. Baumjohann[1,2], J. Untiedt[1], and R.A. Greenwald[3]

[1] Institut für Geophysik der Universität Münster, Corrensstr. 24, D-4400 Münster, Federal Republic of Germany
[2] Max-Planck-Institut für Physik und Astrophysik, Institut für extraterrestrische Physik, D-8046 Garching, Federal Republic of Germany (Present affiliation)
[3] Applied Physics Laboratory, The Johns Hopkins University, Laurel, MD 20707, USA

Abstract. On 2 December 1977, 1600–1700 UT (around 19 MLT) a section of the Harang discontinuity moved westward over northern Scandinavia with a velocity of about 1 km/s, during a disturbed time interval. The westward movement was clearly identified in the IMS Scandinavian Magnetometer Array observations and is consistent with simultaneous STARE electric field measurements. The magnetic measurements showed a marked increase of the overhead current density during the westward movement while the electric field amplitudes stayed at the same level, thus indicating a temporal enhancement of the ionospheric conductivity. The westward movement gave the opportunity to combine subsequently observed two-dimensional distributions of equivalent current vectors (after correction for the magnetic field intensity increase) and electric field vectors into two corresponding patterns fairly extended in the east-west direction and covering the total extent of the most interesting part of the Harang discontinuity region. The electrically defined Harang discontinuity was located 200–300 km to the north of the magnetically defined discontinuity. The combined observational data were used to determine, as far as possible, the ionospheric distributions of height-integrated conductivities, of horizontal height-integrated current density vectors and of field-aligned currents. The results show a reduction of the Hall conductivities and upward Birkeland currents at and around the electrically defined Harang discontinuity. Some horizontal ionospheric current crosses the discontinuity, being diverged northward from the eastward electrojet and joining the westward electrojet, after further counterclockwise rotation.

Key words: Polar ionosphere – Harang discontinuity – Ionospheric electric field – Ionospheric conductivity – Ionospheric and field-aligned currents

Introduction

Today there are two main definitions of the Harang discontinuity in use. In the first case, it is defined as the evening sector separatrix between the two parts of the auroral oval which are dominated by the eastward and westward electrojet, respectively (Fig. 1 a). Because it is very difficult to measure true ionospheric currents, equivalent currents (i.e. horizontal magnetic disturbance vectors observed at the earth's surface and rotated clockwise by 90°) are used in this definition. This corresponds to the work of Harang (1946) who first detected that in the disturbed auroral zone there exists a line which is moderately inclined with respect to circles of magnetic latitude and separates positive disturbances in the magnetic north component B_x to the south and west from negative disturbances to the north and east. This line was named the Harang discontinuity by Heppner (1972). It is not fixed even in a magnetic latitude – magnetic local time coordinate system but may change position rapidly especially in connection with strong magnetic activity. For example, the penetration of the westward electrojet into the evening and afternoon sector during substorms (Rostoker and Kisabeth, 1973; Wiens and Rostoker, 1975) may shift the discontinuity by several hours of local time towards the west. Sometimes such a shift may occur during a fraction of an hour as noted by Heppner (1967) who spoke of discrete jumps of the discontinuity within this context. Note, that the magnetical Harang discontinuity can be defined only if magnetic disturbances are present. If magnetic activity is small it usually terminates at the southern bound-

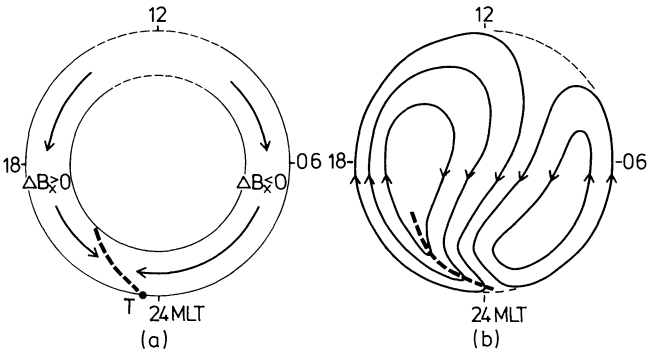

Fig. 1 a and b. Schematic representation of **a** equivalent current flow within the auroral oval (cf. Hughes and Rostoker, 1979) and **b** plasma convection flow within the auroral oval and the polar cap (cf. Heppner, 1977, for example). In each diagram, the *heavy broken line* represents the respectively defined Harang discontinuity. ΔB_x denotes the northward component of the magnetic disturbance field

* *Present address:* Siemens AG, München, Federal Republic of Germany

Offprint requests to: J. Untiedt

ary of the auroral oval near magnetic midnight (cf. point T in Fig. 1a).

In the second case, the Harang discontinuity is defined from the two-cell configuration of the ionospheric electric field **E** at high latitudes (e.g. Heppner, 1977) and denotes the line which separates westward from eastward convection ($\mathbf{E} \times \mathbf{B}/\mathbf{B}^2$) flow in the evening-midnight sector within and near to the auroral oval (Fig. 1b). Usually the flow shows an additional southward component at and near to the discontinuity. The electrical Harang discontinuity has been studied particularly by advanced techniques such as satellite instruments (e.g. Maynard, 1974), incoherent scatter radars (e.g. Banks et al., 1973; Wedde et al., 1977; Horwitz et al., 1978a, b) and coherent twin auroral radar systems like STARE and SABRE (e.g. Nielsen and Greenwald, 1979; Zi and Nielsen, 1982; Waldock et al., 1985). Usually it is situated 1°–2° to the north of the magnetic Harang discontinuity (Kamide and Vickrey, 1983). Like the latter, it is highly dynamic in nature. As magnetic activity increases, the region of predominantly westward electric field which includes the discontinuity narrows and moves to lower latitudes, on average (Maynard, 1974). The velocity of this movement increases with increasing Kp (Nielsen and Greenwald, 1979). The discontinuity generally appears earlier when magnetic activity is higher (Heppner, 1972; Nielsen and Greenwald, 1979; Zi and Nielsen, 1982; Waldock et al., 1985). Most of these features may be understood if the following view suggested by Zi and Nielsen (1982) on the basis of STARE observations is adopted (see also Burrage et al. 1985; Waldock et al., 1985). As magnetic activity increases: (1) the convection flow speeds increase; (2) the polar two-cell flow pattern expands; (3) the morning cell is enlarged with respect to the evening cell; and (4) the whole convection pattern rotates clockwise towards earlier local times.

As pointed out by Kamide (1982), there still exists much ambiguity about how such features like ionospheric horizontal and field-aligned currents, or ionospheric conductivities, change across the discontinuity. For example, three sheets of alternatively directed Birkeland currents have been deduced from the Triad satellite magnetic field observations for the 20–24 MLT sector of the auroral oval, under most conditions, with upward flow in the middle sheet (Iijima and Potemra, 1978; see also Rostoker et al., 1975). During periods when the westward auroral electrojet had intruded deeply into the evening sector, the Triad observations indicated the presence of even more complex field-aligned currents in this sector. On the other hand, Kamide (1978) discussed the possibility, which is also supported by observations, that there is no field-aligned current flow at the Harang discontinuity. He presented a model (cf. also Kamide et al. 1976a, b) in which poleward ionospheric current across the discontinuity region connects the eastward electrojet and the westward electrojet in the pre-midnight sector. Baumjohann et al. (1980) supported such a model by giving qualitative observational evidence for it, but at the same time described in detail a case where the eastward electrojet terminated exclusively by feeding strong and localized upward field-aligned current. Probably these are two extreme opposite possibilities which in most cases will be mixed in some way.

Very little is known about the behaviour of the height-integrated Hall and Pedersen conductivities, Σ_H and Σ_P, respectively. Recently, Kamide and Vickrey (1983), combining observations of the Chatanika incoherent scatter radar and the IMS Alaska meridian chain of magnetometers, found conductivity enhancements only on the poleward side of the electric Harang discontinuity during relatively quiet times and the early stage of a substorm. However, the enhancement surged equatorward extending beyond the discontinuity when the substorm reached the maximum to recovery phase. On the other hand, Baumjohann et al. (1981), after studying a multiple onset substorm over Scandinavia around magnetic midnight, reported that each auroral break-up occurred slightly south of the Harang discontinuity in the region of northwestward-directed electric field vectors. Observation of energetic particle precipitation into the region of the Harang discontinuity (Wedde et al., 1977) suggests a local increase of the ratio Σ_H/Σ_P, whereas Vickrey et al. (1981) found a decrease. Kamide and Vickrey (1983) also deduced a comparatively small conductivity ratio of 1.3 from the Harang discontinuity which they observed.

In view of these ambiguities it seems worthwile to study single cases of occurrences of the discontinuity in greater detail and by different methods of observation. A unique opportunity for such studies is offered by the data set simultaneously acquired over Scandinavia during the years 1977–1979 from the two-dimensional IMS Scandinavian Magnetometer Array (SMA) (Küppers et al., 1979; Maurer and Theile, 1978) and the Scandinavian Twin Auroral Radar Experiment (STARE) (Greenwald et al., 1978). The SMA consisted of more than 30 magnetometer stations, separated by about 100–150 km in northern Scandinavia where the network was most dense. It was mainly operated by the University of Münster and partly by the Technical University of Braunschweig.

The STARE system which is operated by the Max-Planck-Institut für Aeronomie at Katlenburg-Lindau consists of two radars at Malvik in Norway and Hankasalmi in Finland with a common area of observation above the northernmost part of Scandinavia and the neighbouring ocean. The radars are sensitive to electrostatic plasma waves in the auroral E region. These waves, often called irregularities, are produced by the combined effects of the two-stream and gradient drift plasma instabilities (see Greenwald, 1974). Greenwald (1979) has summarized evidence that, in the auroral E layer, the net drift velocity of the irregularities is nearly a pure $\mathbf{E} \times \mathbf{B}$ drift. Hence, the transverse ionospheric electric field vector is orthogonal and proportional to the measured drift velocity vector. Experimental evidence for this relationship has been found by Ecklund et al. (1977), Cahill et al. (1978) and Zanetti et al. (1980). Recently, Nielsen and Schlegel (1983, 1985) compared data of ionospheric electron drift velocities estimated by STARE with data of simultaneous velocity measurements made with the European Incoherent Scatter Facility (EISCAT). The magnitudes of the estimated drift velocities were in agreement with the EISCAT measurements for small velocities ($\lesssim$700 m/s, corresponding to electric fields $\lesssim$35 mV/m), but the authors found the estimates to be increasingly too low as the velocities become larger. The directions of the estimated vectors were in agreement with the EISCAT measurements for all drift magnitudes.

The drift velocities which may be converted to electric field vectors are observed with a temporal resolution of 20 s and a spatial resolution of about 20 km. The area viewed by STARE is located between about 68° and 73° northern geographic latitude and between about 14° and

24° eastern geographic longitude, corresponding to an extent between about 65° and 70° revised corrected geomagnetic latitude Φ_c (Gustafsson, 1970). Because the SMA reaches about $\Phi_c = 67.5°$ at the northernmost coast of Scandinavia, there is only partial overlap between the STARE and the SMA areas of observation. In many cases, there are quite extended gaps in the STARE data which may further diminish the overlap. These gaps result from regions in which the electric field does not exceed the threshold value of about 15–20 mV/m (Cahill et al., 1978) required to excite the plasma instabilities observable by STARE.

It is the purpose of the present paper to describe, for the first time, a single-event study of the Harang discontinuity using two-dimensionally distributed simultaneous data from the SMA and STARE. Our main intention was to estimate the spatial distribution of the height-integrated ionospheric conductivities, of height-integrated horizontal ionospheric currents and of field-aligned currents in the particular case considered. We do not intend to generalize the results from this investigation. As indicated above, the Harang discontinuity is a very dynamic and variable phenomenon so that many and perhaps improved studies of the kind which we are presenting will probably be necessary before general conclusions can be drawn.

In the course of our investigation we detected that the section of the discontinuity which we were able to observe by means of the SMA was a fast travelling phenomenon, moving in the same manner in which a westward travelling surge or in which eastward drifting omega bands will move. In previous studies, this motion was used to superimpose magnetic field distributions consecutively observed by the SMA in order to get snapshots of the westward travelling surge (Inhester et al., 1981; Opgenoorth et al., 1983b) or of eastward travelling omega bands (Gustafsson et al., 1981; André and Baumjohann, 1982; Opgenoorth et al., 1983a) within a field of view much extended in the direction of motion, as compared to the field of view of the SMA. In the present case, the motion was uniquely determinable only from the SMA observations, whereas the STARE data were at least consistent with the hypothesis that the electric field around the Harang discontinuity studied was moving together with the magnetic field. By accepting this obvious hypothesis we were able to reproduce not only a probably realistic extended snapshot of the magnetic field, but also a corresponding snapshot of the electric field distribution around the investigated Harang discontinuity with an east-west extent of about 2000 km equivalent to about 3 h in local time. We consider these extended field distributions to constitute a first interesting result of our study.

The event

In selecting a suitable event for our investigation we required it not to be an exceptional case according to previous experience with SMA and STARE data. Several cases of former observations of the Harang discontinuity by STARE were presented by Nielsen and Greenwald (1979), and the result of a corresponding statistical study based on STARE observations during 18 disturbed days was given by Zi and Nielsen (1982). As concerns SMA data, papers by Baumjohann et al. [1978, their Fig. 4b; cf. also Richmond and Baumjohann (1983) and Murison et al. (1985)], Küppers et al. (1979, their Fig. 9b) and Baumjohann et al. (1980, their Fig. 15) show examples of temporary appearance of the Harang discontinuity at different magnetic local times (which is about UT + 2.5 h in northern Scandinavia) within the evening sector, in connection with enhanced magnetic activity. In most of these examples and other cases not published hitherto, the equivalent current pattern shows a rotational transition from eastward currents in the south over northward currents to northwestward currents in the north. Furthermore, we required that the discontinuity appeared in the region of overlap of the STARE and SMA fields of view and, finally, that the STARE data did not show too many extended gaps (due to the threshold effect mentioned).

The event selected occurred on 2 December 1977 between 1600 and 1700 UT (about 1900 MLT). This is rather early in magnetic local time but, in view of the strong magnetic activity (Kp = 6+ for the time interval 1500–1800 UT and ΣKp = 44 for the UT day), not really exceptional. Note that Zi and Nielsen (1982; cf. also Nielsen and Greenwald, 1979) got an average shift of the discontinuity by about 3 h to earlier local time for ΣKp = 40–50, and that Waldock et al. (1985) gave an average appearance of the discontinuity at 2030 MLT for Kp = 6 and for the SABRE field of view which is located several degrees to the south as compared to northern Scandinavia and therefore may be expected to see the Harang discontinuity later.

To give a first impression on how the Harang discontinuity occurred on 2 December 1977, and what kind of magnetic activity followed, Fig. 2 shows the horizontal magnetic disturbances observed in the Scandinavian region on that day between 1500 and 2300 UT (about 1730 and 0130 MLT) along one of the meridian magnetometer lines of the SMA. The eight stations of this line stretch from $\Phi_c =$ 67.4° (SOY) at the northernmost coast of Norway to $\Phi_c =$ 58.8° (SAU) in southern Finland. The disturbances are defined as deviations from the quiet night level and are given in a system of coordinates and field components which has been particularly designed for the analysis of SMA data and has been named the Kiruna system (Küppers et al., 1979).

As regards coordinates, the Kiruna system is obtained by projecting the Scandinavian part of the curved earth's surface onto a tangential plane centred at the town of Kiruna (67.8° N, 20.4° E in geographic coordinates) which is located at the centre of the most important northern part of the SMA. Then, a Cartesian system of coordinates x_{KI} and y_{KI} is introduced with its origin at Kiruna. The orientation of this system has been chosen in such a way that at Kiruna the y_{KI} axis is tangent to the projection of the line of constant revised corrected geomagnetic latitude running through this place. x_{KI} increases roughly towards the north and y_{KI} increases towards the east. At Kiruna, the x_{KI} axis points 12° west of geographic north. If the third dimension is needed, height is used as the corresponding coordinate. Finally, horizontal components of a magnetic or electric field are transformed in the same way as described by Küppers et al. (1979). For the sake of brevity the magnetic disturbance field component parallel to the x_{KI} axis is usually denoted by A, and the corresponding component parallel to the y_{KI} axis is denoted by B. The Kiruna system will be used exclusively within the present paper. When we mention northerly and westerly directions this will imply that directions parallel to the x_{KI} axis and the y_{KI} axis are being indicated, respectively. Correspond-

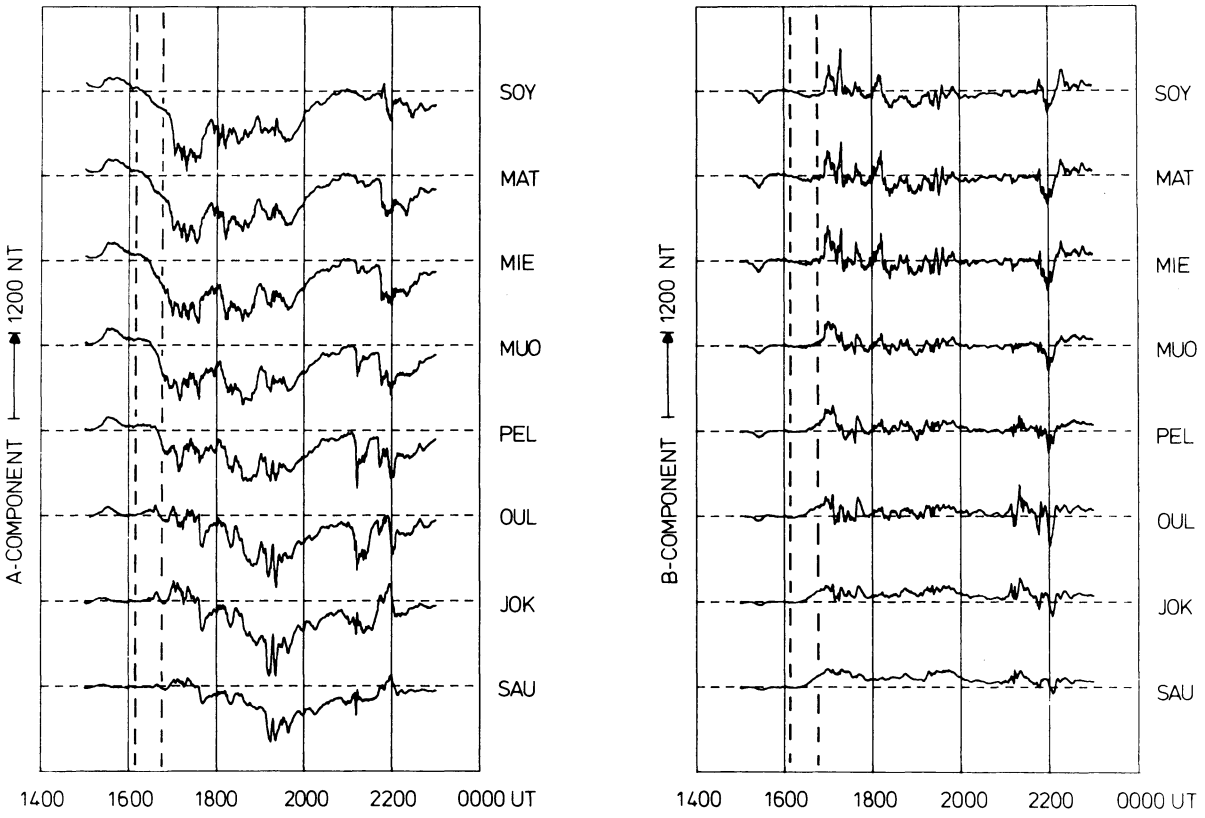

Fig. 2. Geomagnetic disturbances as recorded along one of the meridian magnetometer lines of the IMS Scandinavian Magnetometer Array on 2 December 1977. The *A* and *B* components are effectively directed towards corrected geomagnetic north and east, respectively (cf. Küppers et al., 1979). The revised corrected geomagnetic latitudes (Gustafsson, 1970) of the stations vary from 67.4° (SOY, northernmost Norway) to 58.8° (SAU, southern Finland). The disturbances are defined as deviations from the quiet night level

ingly, *A* and *B* components may be called north and east components, respectively.

As Fig. 2 shows, the event which we studied (cf. vertical broken lines) occurred at the transition from northerly to southerly magnetic disturbances over northern Scandinavia, with mostly moderate intensities of about 100–200 nT. Additionally, the northern stations showed small westerly disturbances, whereas easterly disturbances in middle and southern Finland became relatively strong towards 1700 UT after having been negligible during the first half of the event.

The temporal development of the spatial structure of the magnetic disturbance field throughout the transitional interval is illustrated by a series of four subsequent instantaneous distributions of equivalent current vectors over Scandinavia (Fig. 3). In each case, the simultaneous distribution of electric field vectors as observed by STARE is added. Note that the STARE data have been averaged over 50×50 km^2 areas.

At 1615 UT (Fig. 3, upper left) the whole of northern Scandinavia is still under the eastward electrojet, as indicated by essentially eastward equivalent current vectors and northward electric fields. However, the northernmost coastal magnetometer stations show small but clearly northward-pointing current arrows corresponding to $A \approx 0$. Therefore, it may be anticipated that the magnetic signature of the Harang discontinuity has already reached the northernmost coast of Scandinavia. This is in accord with the predominantly westward current observed by the Norwegian observatory on Bear Island to the north.

At 1628 UT (Fig. 3, upper right) the magnetic signature of the Harang discontinuity (i.e. northward equivalent current vectors) has moved to the south and is now well observed by magnetic stations, stretching in a northwest-southeasterly direction over northern Scandinavia. In the same area, STARE still shows north- to northwestward-directed electric field vectors, whereas at some distance to the north a westward field, i.e. the electric signature of the Harang discontinuity, has appeared. As mentioned above, such a meridional separation between the magnetic and electric signatures of the Harang discontinuity has recently been pointed out by Kamide and Vickrey (1983). Note that there are quite extended gaps in the STARE data. As mentioned above, they result from regions in which the electric field does not exceed the threshold value of about 15–20 mV/m (Cahill et al., 1978). In fact, the northward or northwestward electric fields detected at 1615 UT and 1628 UT have just this intensity, whereas the westward fields at 1628 UT show a somewhat larger magnitude of 25–30 mV/m.

About 10 min later (Fig. 3, lower left) both signatures of the Harang discontinuity are located even further south. In the equivalent current pattern the eastward electrojet in the south and the westward electrojet in the north are well separated with almost no current crossing the Harang discontinuity. The electrical signature of the discontinuity is again displaced to the north, by about 200 km as compared to the magnetic signature, and is indicated by a data gap between northwestward field vectors to the south and southwestward field vectors to the north. It may safely be

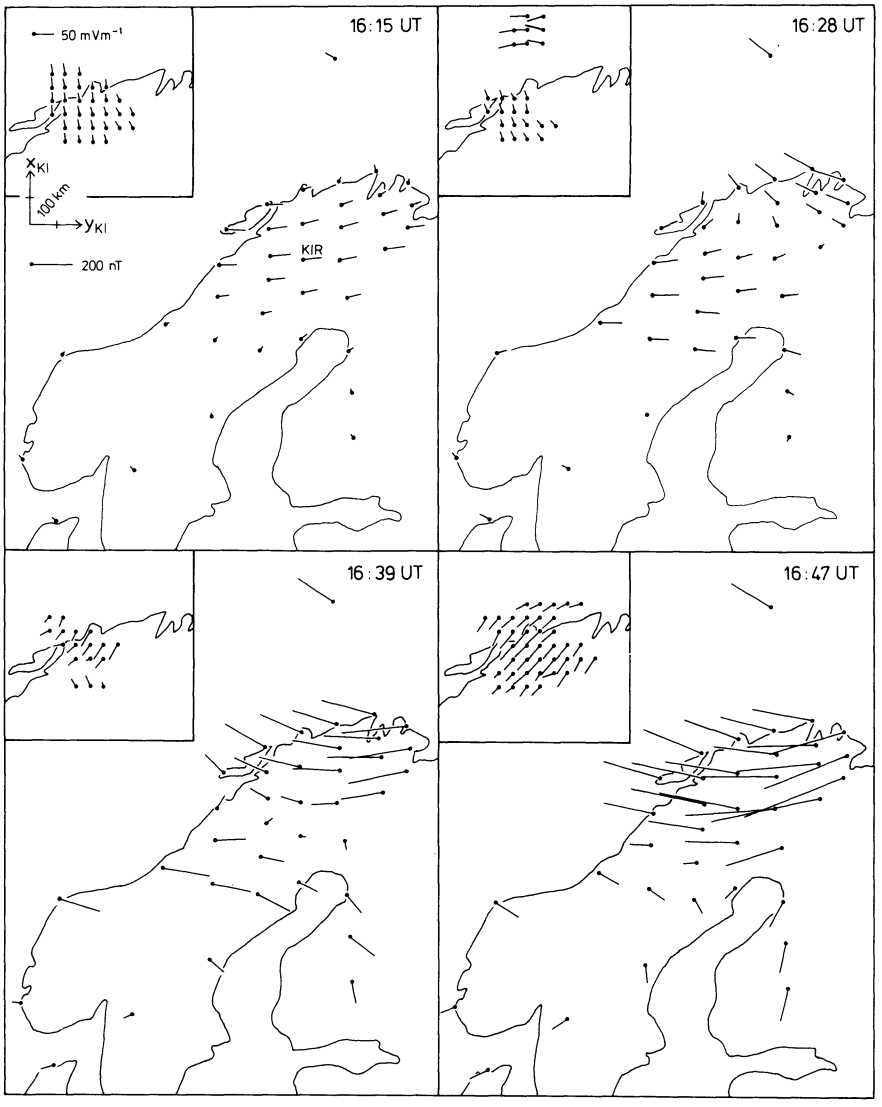

Fig. 3. Distributions of horizontal magnetic disturbance vectors rotated clockwise by 90° (equivalent current vectors) and of ionospheric electric field vectors observed on 2 December 1977. Note that the STARE area of observation is displaced (cf. coast line). Also displaced is the x_{KI}–y_{KI} system of coordinates (for details, see text) shown in the *upper left main panel*. In reality, its origin is located at the magnetic station Kiruna (*KIR* indicated). The directions of its axes coincide with the directions of the *A* and *B* components displayed in Fig. 1. The single magnetic station to the north is the Norwegian permanent observatory on Bear Island

assumed that within this gap the field is mainly westward, with an intensity below threshold. Note that obviously the width of the electrically defined Harang discontinuity has decreased much between 1628 UT and 1639 UT, and that equivalent currents have intensified whereas such an effect can barely be recognized in the STARE data. Probably the southeastward orientation of equivalent current vectors south of the auroral zone indicates an at least partial divergence of the eastward polar electrojet as upward net field-aligned current (cf. Baumjohann et al., 1980, particularly their Fig. 11).

Finally, at 1647 UT (Fig. 3, lower right) an intense westward electrojet is flowing above northern Scandinavia and STARE observes southwestward-directed fields at 35–45 mV/m intensity which in reality may be somewhat larger according to Nielsen and Schlegel (1983).

In summary we may state that between about 1615 UT and 1650 UT the Harang discontinuity, with the electrical and magnetic signatures separated as reported by Kamide and Vickrey (1983), moved from north to south over Scandinavia. At the same time, the character of the equivalent current pattern changed significantly. Whereas early within the time interval eastward electrojet current diverged northward and then joined the northwestward currents to the north after crossing the Harang discontinuity, later the eastward jet turned southward away from the discontinuity.

Generation of extended snapshots of the magnetic and electric fields

These very different characters of the equivalent current patterns (i.e. of the magnetic fields) observed early and late within the time interval mentioned can be reconciled if the subsequent patterns are shifted with respect to each other as shown by Fig. 4. Within this figure, and in the remainder of our paper, only the six equivalent current distributions observed at 5-min distances from 1620 to 1645 UT are used because it turned out that the rest of the magnetic data from this time interval contained effectively redundant information. The shift between any two subsequent current patterns has been adjusted in such a way that current flow within the overlapping parts of the patterns was parallel. Note that generally a similar fitting of equivalent current configurations observed subsequently throughout the course of magnetic substorms will not be possible, with the exception of westward travelling surges etc. (see above). The obvious possibilitiy of such a fitting was an early unexpected result of our study.

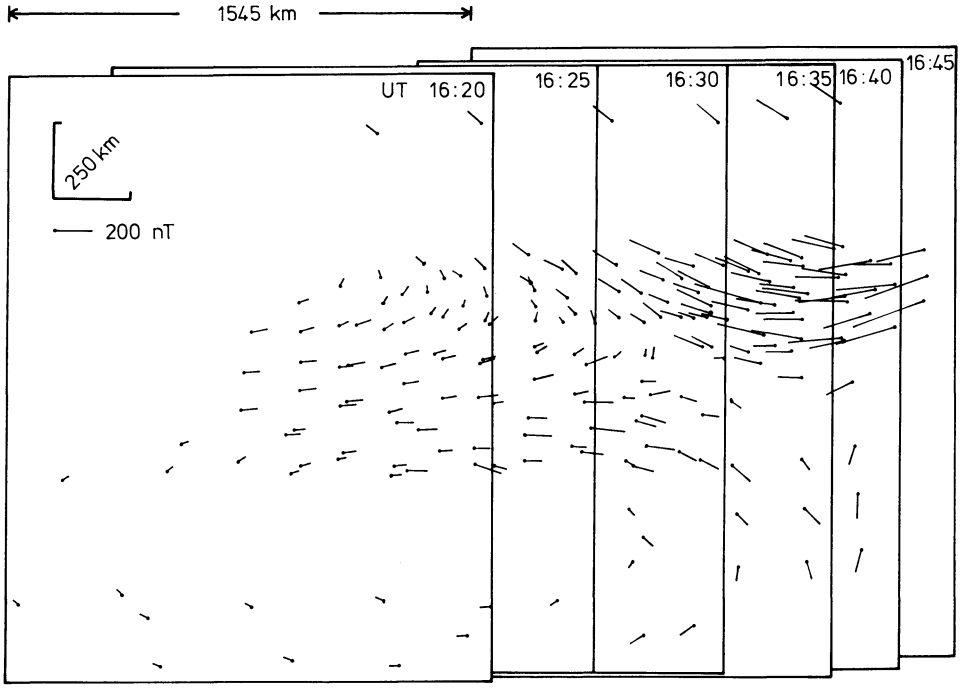

Fig. 4. Extended equivalent current vector distribution generated by properly combining the six corresponding distributions that were observed from 1620 UT to 1645 UT at 5-min intervals. The fit of the different observed patterns was done under the condition that current directions agree in overlapping areas. Frames are identical to those used within Fig. 3 for presentation of the magnetic (equivalent current) data

Figure 4 demonstrates that each one of the equivalent current patterns, observed at 1620 UT, 1625 UT and so on, may be considered to be a different and more and more easterly shifted section from a single extended pattern which becomes obvious in the figure. Conversely, we may state that on 2 December 1977 between 1620 and 1645 UT an extended equivalent current distribution as shown by Fig. 4 moved almost exactly westward over Scandinavia with a speed that varied slightly, as readable from the different values of shift per 5 min, around an average speed of 1.0 km s^{-1} (1,545 km as indicated within the figure divided by 25 min).

The final goal in our magnetic data analysis was the generation of a consistent and uniform version of the current vector field indicated by Fig. 4. However, before accomplishing this we had to undertake one additional step. By shifting the subsequently observed current patterns as described above it was possible to match current directions but not current intensities, within overlapping sections. Obviously, current intensity increased with time, as is also suggested by the sequence of equivalent current patterns shown in Fig. 3. Figure 5 gives the result of a crude determination of this increase which apparently was not constant over the event. For subsequent 5-min intervals, i.e. 1620–1625 UT, 1625–1630 UT, etc., intensification factors were measured for as many station pairs that were nearly coincident after translation as possible. The ratios were calculated from the equivalent current intensities separated by 5-min intervals. As Fig. 5 shows, there is much scatter in the results, possibly indicating that the stations were sensing regimes of eastward, northward and/or westward equivalent currents. From Fig. 5 we have derived average intensification factors 1.14, 1.39, 1.23, 1.03 and 1.20 for the five subsequent 5-min time intervals of the event, respectively.

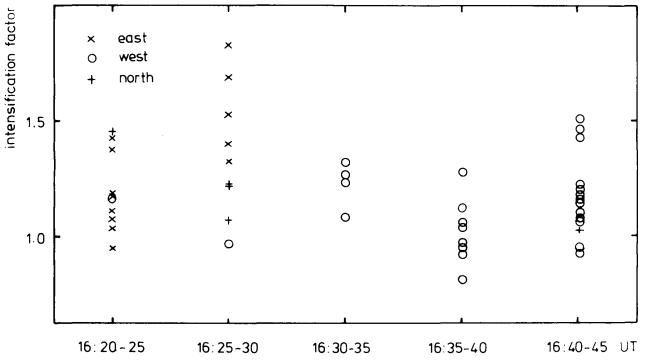

Fig. 5. Intensification factors which describe the increase of intensity of the observed travelling equivalent current system (cf. Fig. 4) over the five consecutive 5-min intervals between 1620 UT and 1645 UT. The factors were estimated by comparing the lengths of equivalent current vectors situated at almost the same location within Fig. 4 but observed 5 min apart

With these factors, we reduced all the equivalent current (i.e. ground magnetic field) data observed at 1620 UT, 1625 UT and so on, to the epoch 1630 UT before finally superposing them. At the same time, we transferred all the superposed data to an equally spaced 100 km × 100 km station grid, by averaging data falling into the same grid cell if necessary. The final result is given by Fig. 6 which is considered to represent the equivalent current distribution which would have been observed over Scandinavia and its western and eastern vicinity on 2 December 1977 at 1630 UT if a corresponding array consisting of about 130 magnetometers extending from $y_{KI} = -1{,}100$ km to $y_{KI} = +1{,}000$ km and $x_{KI} = -1{,}000$ km to $x_{KI} = +700$ km had been available.

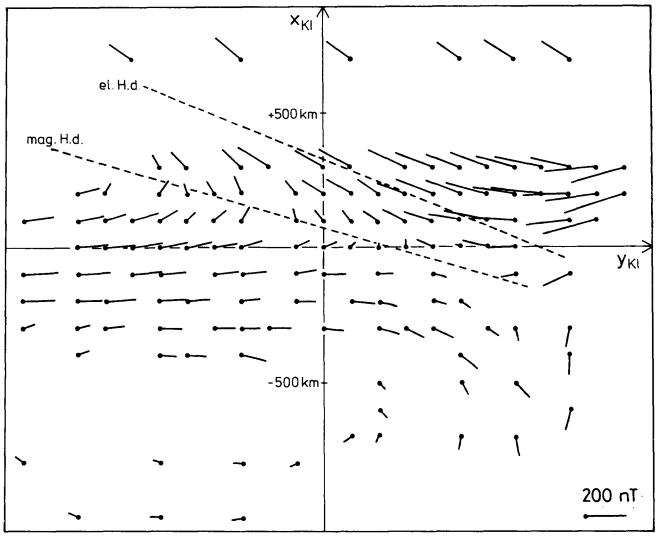

Fig. 6. Distribution of equivalent current vectors at 1630 UT as derived from Fig. 5 by reduction to an equidistant grid of fictitious stations separated by 100 km in both directions and after normalization of current strength to the time 1630 UT (see text). The lines denoted by 'mag. H. d.' and 'el. H. d.' give the locations of the magnetically and electrically defined Harang discontinuities, respectively. The latter discontinuity is transferred from Fig. 7

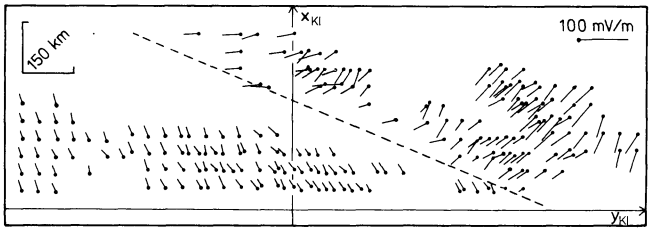

Fig. 7. Extended ionospheric electric field distribution at 1630 UT generated by combining 12 corresponding distributions that were observed consecutively by STARE from 1620 UT to 1645 UT. The composition was done in a similar way to Fig. 4 but under the assumption that the electric field had travelled with the same velocity vector as that deduced from the magnetic observations and applied in Fig. 4. The *dashed line* denotes the estimated locus of the electric signature of the Harang discontinuity (i.e. westward electric field)

This extended snapshot of the equivalent current distribution shows an eastward electrojet intruding into the area along the y_{KI} axis with its centre at about $x_{KI} = -100$ km. It diverges partly towards the north and afterwards northwest joining the continuation of the westward electrojet that intrudes with its centre at about $x_{KI} = +200$ km. The remaining part of the eastward electrojet turns southward within the southeastern section of the area shown. To the southwest, there is equivalent return current to the eastward jet. The locus of the magnetic signature of the Harang discontinuity, i.e. of northward equivalent current, is indicated by a broken line. Whereas it may be anticipated to be continued towards the northwest, it clearly terminates in the southeastern part of the figure at a location probably corresponding to the point T shown within Fig. 1a.

The next objective was to generate a corresponding snapshot of the ionospheric electric field, if possible. However, the area covered by STARE observations is relatively small and often diminished by the presence of data gaps where the electric field is below threshold. Therefore, we were not able to deduce translation vectors from the subsequently observed electric field distributions. On the other hand, it seemed reasonable to assume that the electric field motion was identical to that shown so clearly by the equivalent current (i.e. magnetic field) patterns. Under this assumption, Fig. 7 has been produced by the translation and superposition of twelve 20-s and 50×50 km^2 averages of the electric field distributions observed by STARE between 1620 UT and 1645 UT. We omitted STARE data patterns that showed too much scatter or too extended data gaps. Because we did not find any evidence of a temporal increase of the overall electric field intensity during this period, as we did in the case of the magnetic field, the field intensities are shown as observed.

Again, we consider Fig. 7 to represent the electric field vectors which an earth-based observer would have measured at 1630 UT if he had had a STARE type system with an area of view much extended in the east-west direction. In other words, Fig. 7 shows a snapshot of the moving ionospheric electric field pattern as seen from the earth. Note that it does not give the field in a moving frame of reference.

The electric field vectors shown in Fig. 7 exhibit more scatter than do the equivalent current vectors in Fig. 4. This difference is typically observed if one compares STARE data with ground-based magnetic measurements. Most likely it is due to the fact that the magnetic measurements are made 100 km below the ionosphere and so are subject to spatial filtering of the smaller-scale structures (cf. Ziesolleck et al., 1983).

It may be noted in Fig. 7 that the absence of electric field data in the westward region of the figure makes it difficult to localize the Harang discontinuity, defined by $E_{x_{KI}} = 0$. However, the discontinuity is easily discernible in the eastern part of the figure and we have indicated it by a dashed line. This line has been extended toward the west where it is at least consistent with the existing data. Note that the electrically defined Harang discontinuity is situated 200–300 km to the north of the magnetically defined discontinuity (cf. Fig. 6 above). This result is consistent with previous observations (e.g. Kamide and Vickrey, 1983).

For a later joint interpretation (cf. next section) of the magnetic and electric observations we will need the electric field with sufficient uniformity and with an extension over a larger area so that it is comparable to the equivalent current distribution as given by Fig. 6. Therefore, we fitted the existing data shown in Fig. 7 and did an interpolation and extrapolation where there were no data by using as simple as possible analytic functions $E_{x_{KI}}$ and $E_{y_{KI}}$ depending on x_{KI} and y_{KI} and imposing the additional condition that the determined smooth electric field be curl-free. Furthermore, we assumed that the southward electric field component far north of the STARE field of view is approximately constant, and that the locus of the electric signature of the Harang discontinuity continues as a straight line towards the southeast. We feel the assumption of a more complicated structure for the model electric field pattern – such as an increase of the southward component to the north, or a changing slant of the Harang discontinuity south of the STARE field of view – to be unwarranted for the present purposes.

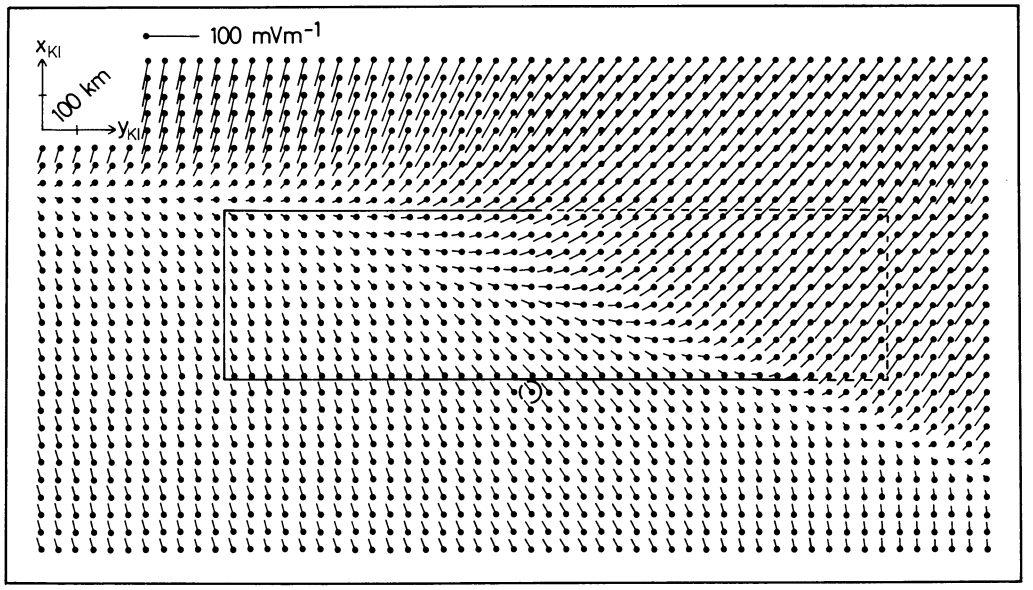

Fig. 8. Similar to Fig. 6 but for the electric field distribution. In this case, the grid spacing is only 50 km, and much smoothing, interpolation and extrapolation has been applied imposing certain conditions (cf. text). The location of the extended STARE area of view (area largely covered by data in Fig. 7) has been marked by a *rectangle*. For clarity, only the origin of the x_{KI}–y_{KI} system (displayed, for example, in Figs. 6 and 7) is indicated by a *circle* (station KIR, cf. Figure 3)

The result is shown on a 50×50 km^2 grid by Fig. 8, with the extended STARE field of view indicated by a rectangle. We think that this is a particularly plausible smoothed representation of the electric field that existed in the region of the Harang discontinuity on 2 December 1977 at 1630 UT. It is both consistent with the STARE observations and also in accord with current knowledge of convection flow at high latitudes (see above). We do not think that much change to the distribution shown in Fig. 8 would be justifiable under these respects, with the exception of the field vectors in the northeastern part of the area where STARE possibly underestimated field intensities (cf. Nielsen and Schlegel, 1983, 1985).

Trial and error determination of ionospheric conductivities and currents

Finally, we tried to find a reasonable ionospheric conductivity distribution which is able to generate Fig. 6 from Fig. 8. As far as the result is unique, it may be considered to represent the conductivity distribution that existed over Scandinavia on 2 December 1977 at 1630 UT. Simultaneously, this conductivity distribution together with the electric field gives true horizontal ionospheric currents, in contrast to equivalent currents, and also the field-aligned currents that are of particular interest in the region of the Harang discontinuity, as discussed above.

We proceeded as described by Baumjohann et al. (1981) who interpreted simultaneously observed SMA and STARE data for three cases of local auroral break-ups, by applying a trial and error method. We assumed a two-dimensional distribution for Σ_H and Σ_P (height-integrated Hall and Pedersen conductivities, respectively) and calculated the ionospheric surface current density $\mathbf{J} = \mathbf{J}_{Hall} + \mathbf{J}_{Ped}$, using the electric field shown by Fig. 8. The divergence of $\mathbf{J}$ gave the field-aligned current density $j_\parallel$. Currents induced within the earth were neglected, in view of the low conductivities found in the crust and upper mantle under northern Scandinavia (Küppers et al., 1979; Jones, 1983). By applying Biot-Savart's law we computed the magnetic field at the ground and finally, by a 90° rotation, equivalent currents. The latter were compared to the observed equivalent current configuration (Fig. 6), and the conductivity distribution was changed until there was adequate agreement between the computed and observed equivalent currents [for more details, see Baumjohann et al. (1981)].

To illustrate and to justify the way in which we proceeded, we present four different models of height-integrated conductivity distributions which, when combined with the electric field distribution given in Fig. 8, yielded model equivalent current patterns on the earth's surface. The conductivity models (Fig. 9) are a selection from a large number of models which gave increasingly better conformity with the observed equivalent current pattern.

In all of the models, we set $\Sigma_H = \Sigma_P = 0$ to the north and to the south of the area covered by electric field vectors in Fig. 8, assuming that it represented the Scandinavian section of the auroral oval and that conductivities outside the oval were negligible. The location of the southern boundary of the adopted auroral oval was suggested by Fig. 6, where the transition from the eastward electrojet to equivalent return currents occurred at about $x_{KI} = -500$ km. If these currents were assumed to be generated by overhead ionospheric currents in a northward electric field this would require negative conductivities which is impossible. The adopted northern boundary of the oval is somewhat arbitrary. However, the exact location of it is of minor influence on the computed equivalent current distribution within the area of interest.

In model 1 (not shown within Fig. 9) we started with uniform oval conductivities and a conductivity ratio $\Sigma_H/\Sigma_P = 2.0$ which is a value typically observed at auroral zone latitudes at nighttime under moderately disturbed conditions (e.g. Banks and Doupnik, 1975; Horwitz et al., 1978a). The values $\Sigma_H = 12$ S and $\Sigma_P = 6$ S were adopted in order to get agreement, as far as possible, between com-

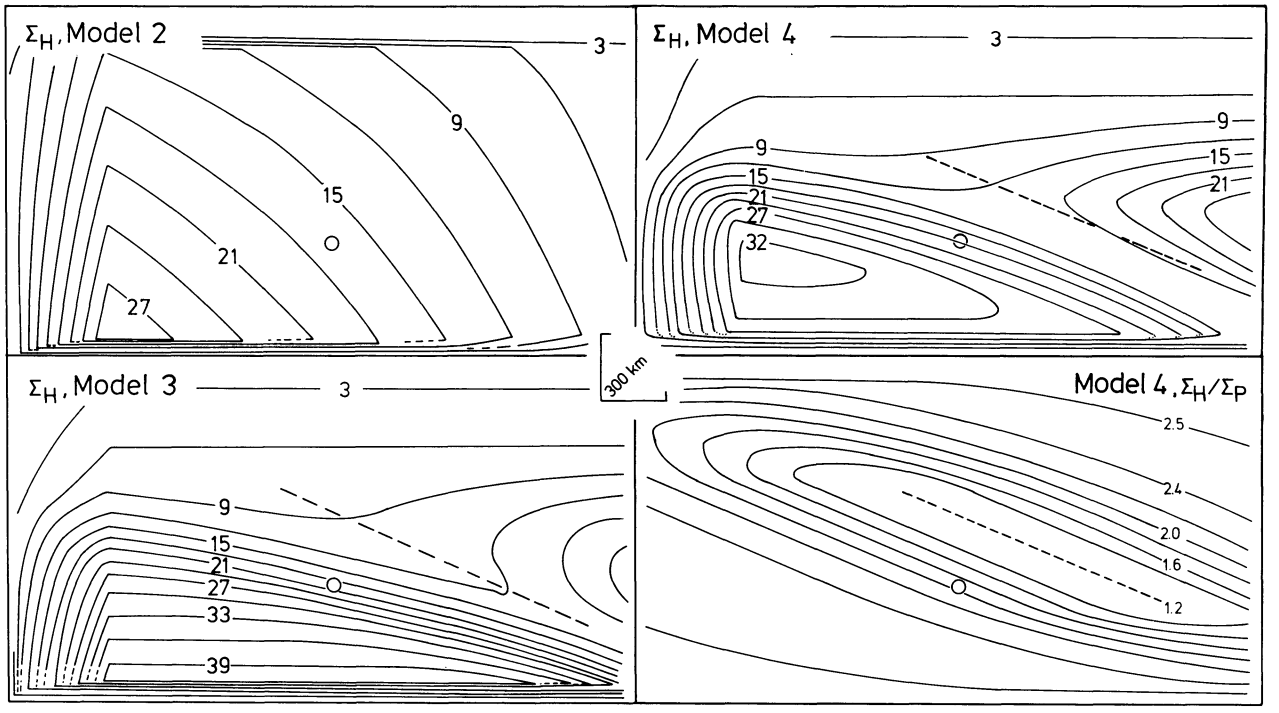

Fig. 9. Different distributions of ionospheric height-integrated conductivities used for modelling the three-dimensional current flow in the Harang discontinuity region by fitting equivalent current distributions calculated for the respective models (cf. Fig. 10) to the observed normalized equivalent current vectors (Fig. 6). For the starting model (model 1; not shown) a uniform conductivity distribution ($\Sigma_H = 12$ S, $\Sigma_P = 6$ S) was used. The Hall conductivity distributions given by isocontours in the *left row* represent intermediate stages (models 2 and 3, $\Sigma_H/\Sigma_P = 2$) while the *upper right panel* gives the Hall conductivity distribution for the final model (model 4). The *lower right panel* gives the spatial distribution of the Hall-to-Pedersen conductivity ratio Σ_H/Σ_P used in model 4. The *dashed lines* denote the electric Harang discontinuity. The centre of the x_{KI}–y_{KI} coordinate system is indicated by a *circle* (as in Fig. 8)

puted equivalent currents (Fig. 10, upper left) and observed equivalent currents within the westward electrojet region. On comparing these currents, one sees that this model is inadequate in that it yields overly small values for the eastward electrojet flow and the equivalent current closure in the southwest.

In order to improve the agreement, the Hall conductivity distribution of model 2 (upper left panel of Fig. 9) has positive Σ_H gradients towards the southwest over most of the model area except for the far west where the gradients are towards the east. These gradients are needed to generate the downward field-aligned currents which provide better equivalent current closure in the southwest. A value of 2 has been retained for the ratio Σ_H/Σ_P. The equivalent current pattern of model 2 is given in the lower left panel of Fig. 10. It shows that the calculated magnetic signature of the Harang discontinuity (dashed line) is located too far to the northeast of the observed one (solid line) and that more westward equivalent current is needed in the central and southern portion of the current pattern. This may be accomplished either by an upward field-aligned current in the east or by more downward field-aligned current in the west. However, since the latter possibility would lead to negative Σ_H values in the far west, Σ_H must increase in the region to the east of the electric signature of the Harang discontinuity.

The conductivity distribution of model 3 includes the above-mentioned modification (Fig. 9, lower left panel, and again $\Sigma_H/\Sigma_P = 2$) and the corresponding calculated equivalent current configuration shown in Fig. 10 (upper right panel) indicates that this indeed leads to the desired results.

The finally adopted Σ_H distribution (model 4), i.e. the final result of our trial and error modelling, is also given in Fig. 9 (upper right). This distribution shows large values around 20–30 S near the eastward end of the eastward electrojet, indicates similar values for the westward jet and gives only 10–15 S in the southern vicinity of the electrically defined Harang discontinuity. Northward of $x_{KI} = 400$ km, Σ_H is below 10 S and decreases steadily towards the north.

In the final conductivity model (model 4) we used a Σ_H/Σ_P distribution with a minimum value of 1.2 at the electrical Harang discontinuity and values increasing above 2.0 away from it (Fig. 9, lower right). We tried such a distribution in view of the above-mentioned observations of Vickrey et al. (1981) and Kamide and Vickrey (1983) and found that it gave slightly better results than a constant ratio and much better results than an assumed increase of Σ_H/Σ_P at the discontinuity. Note that the equivalent current pattern computed from the final conductivity model (Fig. 10, lower right) agrees fairly well with the observed pattern (Fig. 6), and that, in particular, the locations of the magnetically defined Harang discontinuities agree.

The height-integrated ionospheric currents **J** and the field-aligned currents $j_\parallel$ computed for the final conductivity model (model 4) are represented in Fig. 11. Apparently, the northeastward-directed ionospheric currents in the region of the eastward electrojet are fed by downward field-aligned current in the west and at the southern border of the auroral oval, as indicated by crosses in the lower panel of Fig. 11. The currents then partially turn northward and join the westward electrojet and partially flow up magnetic field lines. Most of the westward electrojet current termi-

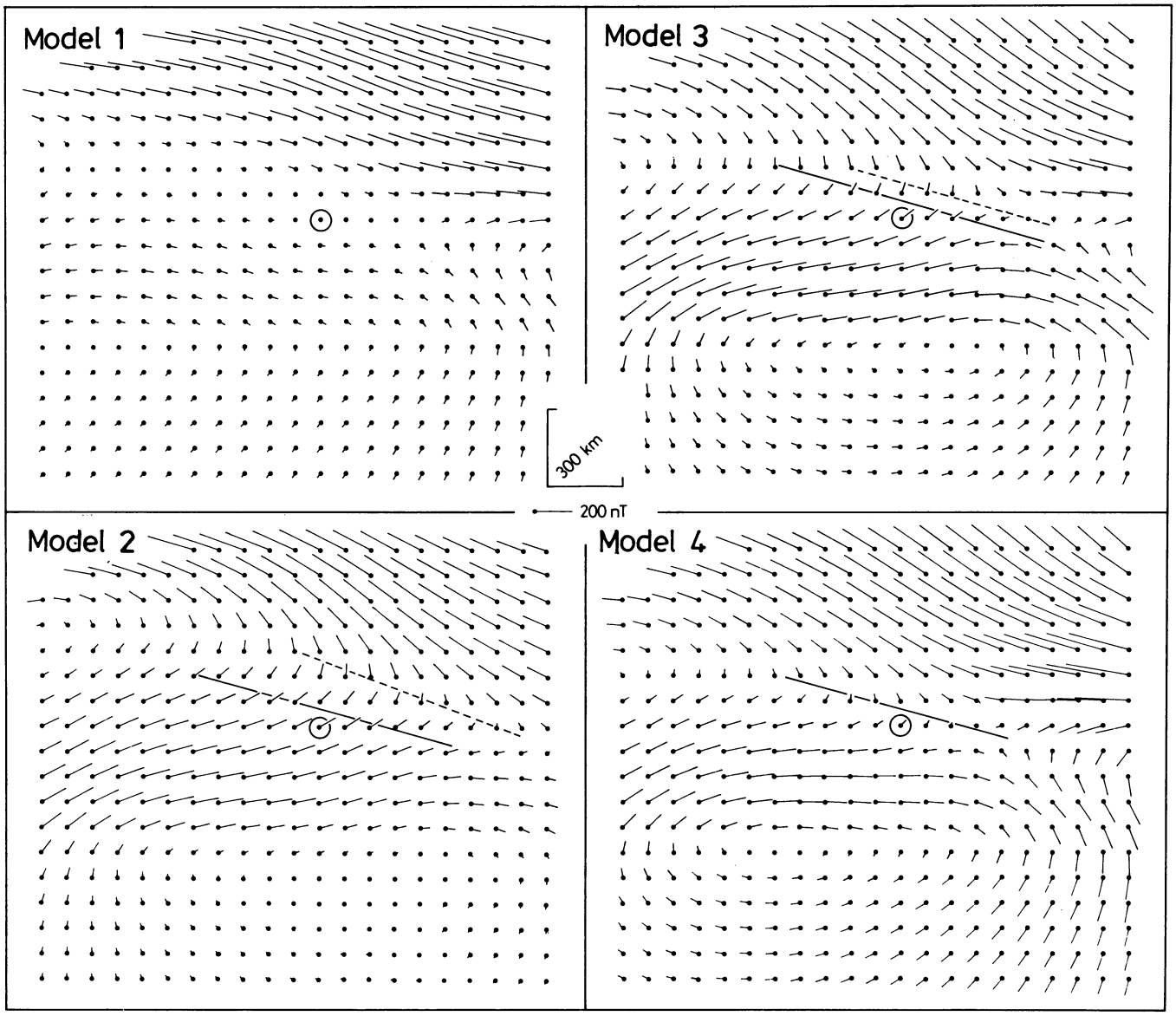

Fig. 10. Model equivalent current vectors on the Earth's surface calculated from the four different conductivity models (cf. Fig. 9 and text) and from the electric field distribution given in Fig. 8. The patterns have to be compared to the observed normalized pattern shown in Fig. 6. Note, that the frames used in Fig. 6 and in this figure are identical. The *circles* bear the same meaning as in Figs. 8 and 9. The *solid lines* denote the observed magnetic Harang discontinuity, whereas the *dashed lines* give the same discontinuity as calculated from the different models. Note, that both lines coincide in the final model (*lower right panel*)

nates in the Harang discontinuity region, particularly near its southeastern part. Altogether, an area of about 600 km × 2,000 km around the electrically defined Harang discontinuity is occupied by upward-flowing Birkeland current of about 1–4 μAm^{-2} intensity.

Because it may be of interest, Fig. 12 shows the field-aligned current distributions estimated separately, by computing the horizontal divergence, from the Hall and from the Pedersen height-integrated currents. It indicates that, in the vicinity of the Harang discontinuity, the Birkeland currents generated by the termination of the eastward electrojet are predominantly from upward-diverging Hall currents; whereas north of the Harang discontinuity, in the region of the westward electrojet, the Birkeland currents are fed mainly by the divergence of Pedersen currents. Note that there are other areas where the field-aligned currents computed separately from the Hall and Pedersen currents partly cancel each other (e.g. to the east of the Harang discontinuity).

Discussion

The first result of our study was the SMA observation of the rapid westward motion of a magnetic field distribution characteristic for the vicinity of the Harang discontinuity. Note that the value of speed determined (about 1.0 kms^{-1}) was large compared to the westward speed corresponding to the earth's rotation (0.16 kms^{-1} at 70° latitude). We feel that this rapid motion corresponds to an early observation by Heppner (1967) (see also Heppner, 1972, p. 115) who studied the local time pattern of geomagnetic disturbance in detail as a function of universal time using data

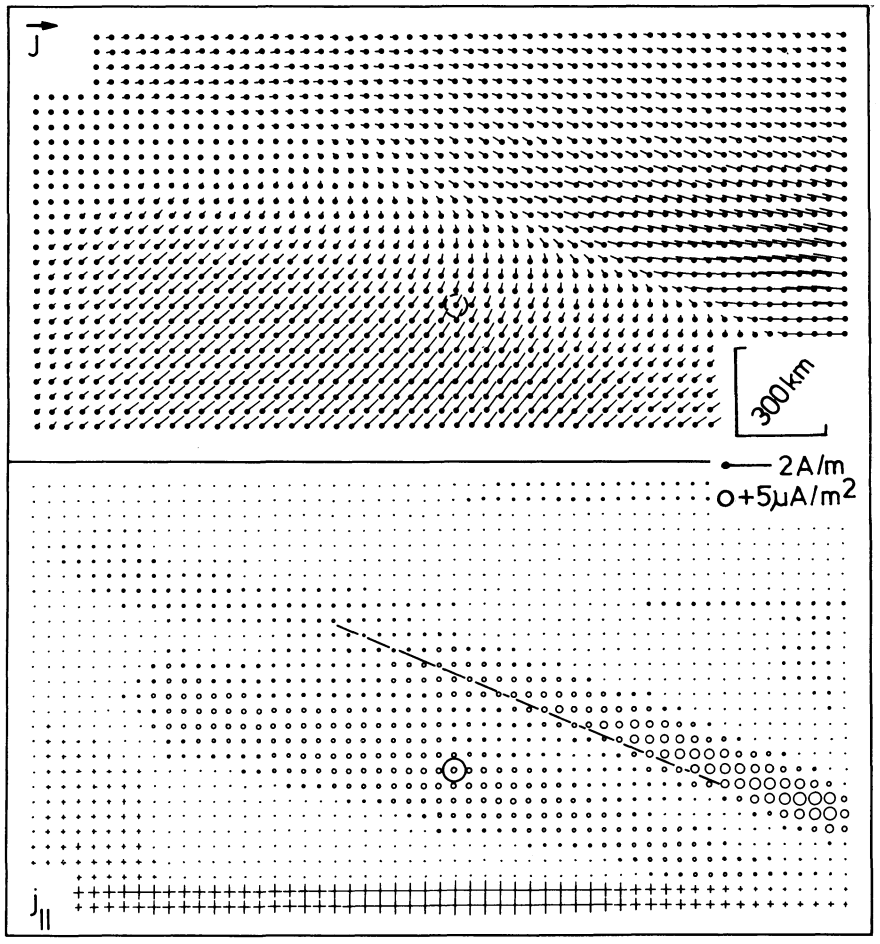

Fig. 11. Ionospheric and field-aligned currents for the final model (model 4, cf. Fig. 9). The *upper panel* gives the height-integrated ionospheric current density. The *lower panel* shows the field-aligned current density (*circles and crosses* denote upward- and downward-directed current flow, respectively). The *two large circles* bear the same meaning as in previous figures. The *straight line* denotes the electric Harang discontinuity

from 25 northern high-latitude observatories for 16 consecutive days in October 1957. Heppner (1967, 1972) found that the transition from + to $-\Delta H$ disturbance (i.e. the magnetic signature of the Harang discontinuity) progressed rather smoothly for most of the time, moving successively from one auroral belt observatory to the next as the earth rotated. However, intermittently superimposed on this general behaviour, discrete jumps occurred in which the discontinuity shifted suddenly (e.g. within 10–20 min) between observatories to an earlier geomagnetic local time. We feel that the magnetic disturbance fields which we observed may have been due to such a jump.

It should be stressed that our conclusions about westward motion have been drawn primarily from the magnetic data. On the basis of the STARE data alone, it was impossible to deduce a westward drift velocity. This is probably due to the limited longitudinal extent of the STARE viewing area, the presence of data gaps and the afore-mentioned greater variability of the STARE data. We have assumed that the STARE observations had been produced by a fixed electric field pattern which moved westward with the velocity of the disturbed magnetic field pattern. Using this assumption, we obtained an extended east-west pattern of the electric field (Fig. 7) in which the locus of the signature of the Harang discontinuity is rotated slightly clockwise from the magnetic (Kiruna system) east-west direction. This inclination leads to a southward motion of the discontinuity as observed between the consecutive STARE plots throughout the event (cf. Fig. 3).

At first glance there appears to be a disagreement between these results and the results of Nielsen and Greenwald (1979) who found that the Harang discontinuity was essentially east-west aligned in the STARE plots that they studied. However, it should be noted that the geographic system of coordinates which they used is rotated by 12° with respect to the magnetically oriented Kiruna system in which we present our results. Therefore, a Harang discontinuity which is exactly east-west aligned in the system used by Nielsen and Greenwald (1979) (an example of such a case is displayed in their Fig. 2) will be rotated 12° clockwise from the y_{KI} axis if it is transferred to our present system of coordinates. This is in essential agreement with our observations and it is only through our ability to overlap numerous magnetic field patterns that we are led to our conclusion of a westward movement of the discontinuity.

The final major results of our study are the distributions of Σ_H, **J** and $j_\parallel$ given by Fig. 9 (upper right panel) and by Fig. 11, respectively. It is important to ask how well-determined or unique these distributions are. This question may be split into three questions. How reliable is the finally adopted electric field shown by Fig. 8 as compared to Fig. 7, and how much would corresponding possible changes within Fig. 8 influence our final results? How far does the trial and error method that was applied give a unique solution?

Regarding the first two questions, the immediate vicinity of the electrically defined Harang discontinuity is most im-

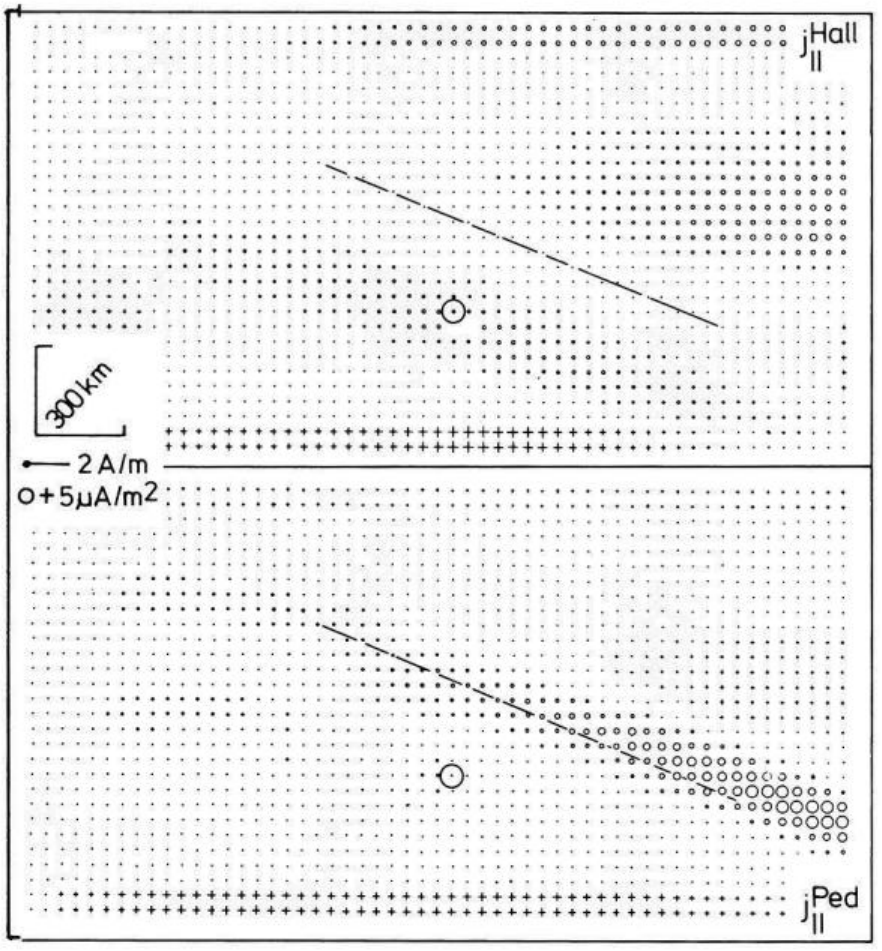

Fig. 12. Field-aligned currents as in Fig. 11, but separately computed from the divergence of the Hall and Pedersen currents, respectively. Otherwise as Fig. 11. Note that the total field-aligned currents shown in Fig. 11 (*lower panel*) are equal to the sum of $j_{\parallel}^{\text{Hall}}$ and $j_{\parallel}^{\text{Ped}}$

portant. Here, the extended STARE data set (Fig. 7) shows large gaps. In our interpolation and regression analysis, we filled these gaps with an electric field that had a constant component parallel to the discontinuity, directed approximately northwestward, and a smooth zero transition in the perpendicular component, with the latter component being constant at constant distance from the discontinuity, in a first approximation. This is in accord with the condition that the electric field be curl-free or, with the equivalent condition, that the convection field be source-free. After a first glance at Fig. 7 it may be asked why it should not be possible, for example, to assume $\mathbf{E}=0$ at the Harang discontinuity. However, consideration of the two equivalent conditions mentioned shows that this would lead to improbable small-scale electric field structure and to an improbable convection flow not consistent with the generally accepted pattern indicated in Fig. 1b, because convection would not be allowed to cross the Harang discontinuity. In the northeastern part of Fig. 8 the electric field vectors reach a magnitude of almost 50 mVm^{-1}. Such large electric fields observed by STARE may have been underestimated as shown by Nielsen and Schlegel (1983, 1985), whereas the field directions remain reliable. If we increase the field strengths correspondingly and simultaneously keep or Σ_H/Σ_P ratios, all Σ_H values in the northeastern part of Fig. 9 (upper right panel) should be reduced by the same factors. On the other hand, $\mathbf{J}$ and $j_{\parallel}$ as shown by Fig. 11 would remain unchanged. Of course, second-order changes of the electric field distribution shown in Fig. 8 would everywhere be possible. However, such minor changes would not give results markedly different from those shown within Fig. 9 (upper right panel) and Fig. 11.

Addressing the third question, we found that the height-integrated Hall conductivities may be changed by up to about 10% as compared to our final model conductivity values without leading to noticeable effects on the equivalent current pattern on the ground. On the other hand, the computed equivalent currents are rather insensitive to the height-integrated Pedersen conductivities. As indicated above, constant ratios Σ_H/Σ_P with values between about 1.5 and 2.5 give almost the same results, and the results are only slightly better for the distribution of Σ_H/Σ_P shown in Fig. 9 (lower right panel). Those results shown in Fig. 11 that we consider to be the most important – namely currents crossing the Harang discontinuity towards the north and upward Birkeland currents in its vicinity – will remain untouched by all such changes of conductivity.

It should be mentioned that some noticeable differences remained between the calculated equivalent current vectors of our final conductivity model and the observed vectors in the far west and in the northeast. They could not be eliminated since the east-west extension of the model ionosphere was limited to about 3000 km. Presumably the region of downward field-aligned current feeding the eastward electrojet in the west – due to the conductivity increase towards the east – was, in reality, extended several hundreds of kilometres more to the west than indicated by our model. Similarly, the region of increasing conductivi-

ty east of the Harang discontinuity may actually be located even further to the east.

Very recently, M. Segatz from the University of Münster developed quite another method for the determination of the Σ_H distribution from jointly observed SMA and STARE data, under the assumption of a given Σ_H/Σ_P distribution (personal communication). The method is based on the solution of a first-order differential equation for Σ_H. Segatz applied this method to the present data set and found essentially the same results as given above, namely high Σ_H values in the termination region of the eastward electrojet and the coexistence of northward and upward diverging ionospheric currents at the location of the electrically defined Harang discontinuity (personal communication). We feel that this also gives further support to the particular trial and error method which was applied in the present case as well as in previous studies (e.g. Baumjohann et al., 1981; Inhester et al., 1981; Opgenoorth et al., 1983b).

Some readers may ask why we did not make use of magnetic vertical component data that also existed. Such data can be reconstructed almost perfectly from the distribution of the two horizontal components (i.e. of equivalent current vectors) if the latter are observed over a densely spaced and extended two-dimensional array, and if the effects of currents induced within the earth may be neglected. Both conditions were fulfilled in our case [as regards the second condition, cf. Küppers et al. (1979)]. Therefore, inclusion of the vertical component would almost not have given additional information and, accordingly, we omitted such data.

Since the magnetic measurements showed a marked increase of the overhead current density during the westward movement while the electric field amplitudes remained essentially at the same level, we conclude that the current increase was due to a temporal enhancement of the total overhead conductivity distribution. We modelled the three-dimensional current flow in the vicinity of the Harang discontinuity by fitting an equivalent current configuration which had been generated by the superposition of subsequently observed and suitably normalized data. Since the total overhead conductivity distribution presumably increased with time and led to the equivalent current increase given by the intensification factors shown in Fig. 5, the isocontour values of the ionospheric conductivity distribution of the final model (Fig. 9, upper right panel) have to be considered to be representative of the time interval around 1630 UT. For other time intervals the conductivities have to be multiplied with normalization factors as indicated by Fig. 5.

Basically, the three-dimensional current flow pattern in and near to the Harang discontinuity on 2 December 1977 which we finally obtained in our study (Fig. 11) corresponds to the concept given by, for example, Baumjohann (1983). Towards the eastern end of the Harang discontinuity, the eastward and the westward electrojet partially terminate by feeding upward field-aligned currents slightly to the south and north of the Harang discontinuity, respectively. The remainder of the eastward electrojet turns northward in this region and joins the westward electrojet.

The model which we obtained may also shed some light upon the Pedersen current circuit in the Harang discontinuity region. This current, which is fed by downward field-aligned current in the south and northeast, diverges upward in a narrow zone which is only a few hundreds of kilometres wide. The zone is colocated with the electric, not with the magnetic, Harang discontinuity (cf. Fig. 6 and Fig. 12, lower panel). This may be considered as additional evidence for the view that the electric Harang discontinuity is the more fundamental demarcation line compared to the magnetic Harang discontinuity.

The existence and intensity of upward field-aligned current in the Harang discontinuity region may depend on how abruptly the horizontal ionospheric electric fields turn counterclockwise from north to south and on how much the conductivity is reduced in the Harang discontinuity. We feel that such different viewpoints as those given by Kamide (1978) – possibility of a non-existence of field-aligned currents in the Harang discontinuity in certain cases – and by Rostoker et al. (1975) or Iijima and Potemra (1978) – importance of field-aligned current in this region – may easily be reconciled under such aspects.

Acknowledgements. The magnetic observations were performed in cooperation with the Aarhus University, the Royal Institute of Technology at Stockholm, the Finnish Meteorological Institute at Helsinki, the University of Bergen, the Geophysical Observatory at Sodankylä, the Kiruna Geophysical Institute, the University of Oulu and the University at Tromsö. The STARE radars are operated with ELAB and the Norwegian Technical University at Trondheim and the Finnish Meteorological Institute at Helsinki. We thank these institutions and all members of the former magnetometer group at the University of Münster and the STARE group at the MPAE for their support. We would also like to thank St. Berger from the University at Tromsö and H. Maurer from the Technical University of Braunschweig for supplying us with magnetic data from the permanent observatory on Bear Island and from the Braunschweig IMS magnetometer chain, respectively. The magnetometer array observations and part of the work by W. Baumjohann were supported by grants from the Deutsche Forschungsgemeinschaft. The effort of R.A. Greenwald was supported by an NSF grant of the Division of Atmospheric Sciences.

Our sincere thanks go also to three unknown referees who sent us extended and well-founded critical but very helpful comments on the first version of this paper.

References

André, D., Baumjohann, W.: Joint two-dimensional observations of ground magnetic and ionospheric electric fields associated with auroral currents. 5. Current system associated with eastward drifting omega bands. J. Geophys. **50**, 194–201, 1982

Banks, P.M., Doupnik, J.R.: A review of auroral zone electrodynamics deduced from incoherent scatter radar observations. J. Atmos. Terr. Phys. **37**, 951–972, 1975

Banks, P.M., Doupnik, J.R., Akasofu, S.-I.: Electric field observations by incoherent scatter radar in the auroral zone. J. Geophys. Res. **78**, 6607–6622, 1973

Baumjohann, W.: Ionospheric and field-aligned current systems in the auroral zone: A concise review. Adv. Space Res. **2**, No. 10, 55–62, 1983

Baumjohann, W., Greenwald, R.A., Küppers, F.: Joint magnetometer array and radar backscatter observations of auroral currents in northern Scandinavia. J. Geophys. **44**, 373–383, 1978

Baumjohann, W., Untiedt, J., Greenwald, R.A.: Joint two-dimensional observations of ground magnetic and ionospheric electric fields associated with auroral zone currents. 1. Three-dimensional current flows associated with a substorm-intensified eastward electrojet. J. Geophys. Res. **85**, 1963–1978, 1980

Baumjohann, W., Pellinen, R.J., Opgenoorth, H.J., Nielsen, E.: Joint two-dimensional observations of ground magnetic and ionospheric electric fields associated with auroral zone currents: Current systems associated with local auroral break-ups. Planet. Space Sci. **29**, 431–447, 1981

Burrage, M.D., Waldock, J.A., Jones, T.B., Nielsen, E.: Joint STARE and SABRE radar auroral observations of the high-latitude ionospheric convection pattern. Nature **316**, 133–135, 1985

Cahill, Jr., L.J., Greenwald, R.A., Nielsen, E.: Auroral radar and rocket double-probe observations of the electric field across the Harang discontinuity. Geophys. Res. Lett. **5**, 687–690, 1978

Ecklund, W.L., Balsley, B.B., Carter, D.A.: A preliminary comparison of F region plasma drifts and E region irregularity drifts in the auroral zone. J. Geophys. Res. **82**, 195–197, 1977

Greenwald, R.A.: Diffuse radar aurora and the gradient drift instability. J. Geophys. Res. **79**, 4807–4810, 1974

Greenwald, R.A.: Studies of currents and electric fields in the auroral zone ionosphere using radar auroral backscatter. In: Dynamics of the magnetosphere, S.-I. Akasofu, ed.: pp 213–248. Dordrecht: D. Reidel, 1979

Greenwald, R.A., Weiss, W., Nielsen, E., Thomson, N.R.: STARE: A new radar auroral backscatter experiment in northern Scandinavia. Radio Sci. **13**, 1021–1039, 1978

Gustafsson, G.: A revised corrected geomagnetic coordinate system. Ark. Geofys. **5**, 595–617, 1970

Gustafsson, G., Baumjohann, W., Iversen, I.: Multi-method observations and modelling of the three-dimensional currents associated with a very strong Ps6 event. J. Geophys. **49**, 138–145, 1981

Harang, L.: The mean field of disturbance of polar geomagnetic storms. Terr. Mag. Atmos. Electr. **51**, 353–380, 1946

Heppner, J.P.: High latitude magnetic disturbances (A brief review with initial results from motion picture presentation). In: Aurora and airglow, B.M. Mc Cormac, ed.: pp 75–92. New York: Reinhold, 1967

Heppner, J.P.: The Harang discontinuity in auroral belt ionospheric currents. Geofys. Publ. **29**, 105–120, 1972

Heppner, J.P.: Empirical models of high-latitude electric fields. J. Geophys. Res. **82**, 1115–1125, 1977

Horwitz, J.L., Doupnik, J.R., Banks, P.M.: Chatanika radar observations of the latitudinal distributions of auroral zone electric fields, conductivities, and currents. J. Geophys. Res. **83**, 1463–1481, 1978a

Horwitz, J.L., Doupnik, J.R., Banks, P.M., Kamide, Y., Akasofu, S.-I.: The latitudinal distributions of auroral zone electric fields and ground magnetic perturbations and their response to variations in the interplanetary magnetic field. J. Geophys. Res. **83**, 2071–2084, 1978b

Hughes, T.J., Rostoker, G.: A comprehensive model current system for high-latitude magnetic activity – I. The steady state system. Geophys. J.R. Astron. Soc. **58**, 525–569, 1979

Iijima, T., Potemra, T.A.: Large-scale characteristics of field-aligned currents associated with substorms. J. Geophys. Res. **83**, 599–615, 1978

Inhester, B., Baumjohann, W., Greenwald, R.A., Nielsen, E.: Joint two-dimensional observations of ground magnetic and ionospheric electric fields associated with auroral zone currents. 3. Auroral zone currents during the passage of a westward travelling surge. J. Geophys. **49**, 155–162, 1981

Jones, A.G.: The electrical structure of the lithosphere and asthenosphere beneath the Fennoscandian shield. J. Geomagn. Geoelectr. **35**, 811–827, 1983

Kamide, Y.: On current continuity at the Harang discontinuity. Planet. Space Sci. **26**, 237–244, 1978

Kamide, Y.: The relationship between field-aligned currents and the auroral electrojets: A review. Space Sci. Rev. **31**, 127–243, 1982

Kamide, Y., Akasofu, S.-I., Brekke, A.: Ionospheric currents obtained from the Chatanika radar and ground magnetic perturbations at the auroral latitude. Planet. Space Sci. **24**, 193–201, 1976a

Kamide, Y., Vickrey, J.F.: Variability of the Harang discontinuity as observed by the Chatanika radar and the IMS Alaska magnetometer chain. Geophys. Res. Lett. **10**, 159–162, 1983

Kamide, Y., Yasuhara, F., Akasofu, S.-I.: A model current system for the magnetospheric substorm. Planet. Space Sci. **24**, 215–222, 1976b

Küppers, F., Untiedt, J., Baumjohann, W., Lange, K., Jones, A.G.: A two-dimensional magnetometer array for ground-based observations of auroral zone electric currents during the International Magnetospheric Study (IMS). J. Geophys. **46**, 429–450, 1979

Maurer, H., Theile, B.: Parameters of the auroral electrojet from magnetic variations along a meridian. J. Geophys. **44**, 415–426, 1978

Maynard, N.C.: Electric field measurements across the Harang discontinuity. J. Geophys. Res. **79**, 4620–4631, 1974

Murison, M., Richmond, A.D., Matsushita, S.: Estimation of ionospheric electric fields and currents from a regional magnetometer array. J. Geophys. Res. **90**, 3525–3530, 1985

Nielsen, E., Greenwald, R.A.: Electron flow and visual aurora at the Harang discontinuity. J. Geophys. Res. **84**, 4189–4200, 1979

Nielsen, E., Schlegel, K.: A first comparison of STARE and EISCAT electron drift velocity measurements. J. Geophys. Res. **88**, 5745–5750, 1983

Nielsen, E., Schlegel, K.: Coherent radar Doppler measurements and their relationship to the ionospheric electron drift velocity. J. Geophys. Res. **90**, 3498–3504, 1985

Opgenoorth, H.J., Oksman, J., Kaila, K.U., Nielsen, E., Baumjohann, W.: Characteristics of eastward drifting omega bands in the morning sector of the auroral oval. J. Geophys. Res. **88**, 9171–9185, 1983a

Opgenoorth, H.J., Pellinen, R.J., Baumjohann, W., Nielsen, E., Marklund, G., Eliasson, L.: Three-dimensional current flow and particle precipitation in a westward travelling surge (observed during the Barium – GEOS rocket experiment). J. Geophys. Res. **88**, 3138–3152, 1983b

Richmond, A.D., Baumjohann, W.: Three-dimensional analysis of magnetometer array data. J. Geophys. **54**, 138–156, 1983

Rostoker, G., Kisabeth, J.L.: Response of the polar electrojets in the evening sector to polar magnetic substorms. J. Geophys. Res. **78**, 5559–5571, 1973

Rostoker, G., Armstrong, J.C., Zmuda, A.J.: Field-aligned current flow associated with intrusion of the substorm-intensified westward electrojet into the evening sector. J. Geophys. Res. **80**, 3571–3579, 1975

Vickrey, J.F., Vondrak, R.R., Matthews, S.J.: The diurnal and latitudinal variation of auroral zone ionospheric conductivity. J. Geophys. Res. **86**, 65–75, 1981

Waldock, J.A., Jones, T.B., Nielsen, E.: Mean auroral E-region plasma convection patterns measured by SABRE. Nature **313**, 204–206, 1985

Wedde, T., Doupnik, J.R., Banks, P.M.: Chatanika observations of the latitudinal structure of electric fields and particle precipitation on November 21, 1975. J. Geophys. Res. **82**, 2743–2751, 1977

Wiens, R.G., Rostoker, G.: Characteristics of the development of the westward electrojet during the expansive phase of magnetospheric substorms. J. Geophys. Res. **80**, 2109–2128, 1975

Zanetti, Jr., L.J., Arnoldy, R.L., Cahill, Jr., L.J., Behm, D.A., Greenwald, R.A.: Comparative rocket observations of ionospheric electric fields in the auroral oval. Space Sci. Instr. **5**, 183–196, 1980

Zi, M., Nielsen, E.: Spatial variation of electric fields in the high-latitude ionosphere. J. Geophys. Res. **87**, 5202–5206, 1982

Ziesolleck, Ch., Baumjohann, W., Brüning, K., Carlson, C.W., Bush, R.I.: Comparison of height-integrated current densities derived from ground-based magnetometer and rocket-borne observations during the Porcupine F 3 and F 4 flights. J. Geophys. Res. **88**, 8063–8072, 1983

Received August 1, 1984; revised version November 14, 1985
Accepted November 18, 1985